Control of plasmas for production of ultraslow antiproton beams

N. Kuroda[*], H.A. Torii[†], M. Shibata[*], Y. Nagata[†], D. Barna[**], D. Horváth[**], M. Hori[‡], J. Eades[§], A. Mohri[*], K. Komaki[†] and Y. Yamazaki[*,†]

[*]*RIKEN, 2-1 Hirosawa, Wako-shi, Saitama, 351-0198, Japan*
[†]*Institute of Physics, University of Tokyo, 3-8-1 Komaba, Meguro-ku, Tokyo, 153-8902, Japan*
[**]*KFKI Research Institute of Particle and Nuclear Physics, H-1525 Budapest, Hungary*
[‡]*CERN, CH-1211 Genève, Switzerland*
[§]*Department of Physics, University of Tokyo, 7-3-1 Hongo, Bunkyo-ku, Tokyo, 113-0033, Japan*

Abstract. To produce ultraslow antiproton beams, decelerated antiprotons were captured in an electro-magnetic trap and cooled by collisions with preloaded electrons. This electron cooling feature was nondestructively monitored by measurement of electrostatic oscillations of the confined electron plasma. The radial distribution of the plasma was controlled for efficient cooling and extraction by utilizing rotating wall field technique.

Keywords: antiproton, non-neutral plasma, multiring trap
PACS: 39.10.+j, 52.27.Jt, 52.35.Fp

INTRODUCTION

The preparation of a large number of antiprotons at extremely low energy is an important step to the study of the initial process of antiprotonic atom ($\bar{p}A^+$) formation [1], to the high precision spectroscopy of $\bar{p}A^+$ [2], to the collision dynamics in the ionization of atoms by antiprotons [3], to the nuclear surface structure via antiprotonic atom formation and annihilation [4, 5], and to the synthesis and spectroscopy of antihydrogen atom[6]. Such exotic atoms can only be efficiently synthesized from component particles at eV and lower energies. The ASACUSA (Atomic Spectroscopy And Collisions Using Slow Antiprotons) collaboration prepared ultraslow antiproton source by the sequential combination of the CERN Antiproton Decelerator (AD), the radio frequency quadrupole decelerator (RFQD), and MUSASHI (Monoenergetic Ultra-Slow Antiproton Source for High-precision Investigation).

The AD at CERN cools and decelerates antiprotons with 2.7 GeV in kinetic energy to 5.3 MeV by stochastic and electron cooling techniques, and ejects them every 84 s with the pulse width of 90 ns, containing 2–3 $\times 10^7$ particles. For further deceleration, we used the RFQD which reduced the 5.3 MeV antiproton beam energy around 110 keV. Some 5×10^6 antiprotons transmitted from the RFQD lost their energy, $\sim$ 100 keV by passing through vacuum isolation foils, which is two 90 μg/cm^2 polyethtlenterephtalate (PET) foils located in front of the MUSASHI (see Fig. 1).

As shown in Fig.1, MUSASHI is composed of two parts, a multiring electrode trap (MRT) [7] housed in 2.5 T magnetic field by a superconducting solenoid and a transport

CP793 *Physics with Ultra Slow Antiproton Beams*
edited by Yasunori Yamazaki and Michiharu Wada

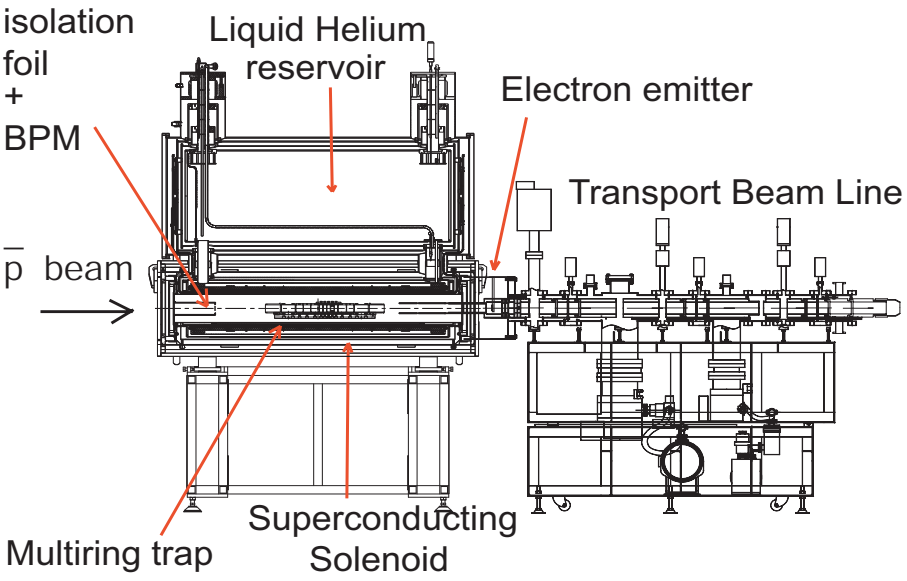

FIGURE 1. A drawing of MUSASHI.

beam line for ultraslow antiproton beams [8]. Antiprotons were captured in the MRT, and then cooled via collisions with preloaded electrons [9]. About 1.2×10^6 among the captured antiprotons at the maximum could be stored in the MRT for periods of 10 min or more [10]. After the cooling, antiprotons were extracted to the field free region via the transport beam line.

In this experiment, we developed a nondestructive plasma diagnostic technique for the study of cooling process of energetic antiprotons by an electron plasma, and also developed the control technique of the radial distribution of plasma and/or charged particle cloud in the MRT for the efficient capture and extraction of antiprotons.

EXPERIMENT

Multiring electrode trap

The MRT consists of 14 ring electrodes as shown in Fig. 2. By applying a proper voltage (like as Fig. 3(a)) on each electrode, F1, FH2, FH1, BH1, S, BH2, and B1 (Fig.2), an electrostatic potential

$$\phi(\rho,z) = -V_0 \frac{\rho^2 - 2z^2}{2L^2 + R^2} + \delta, \tag{1}$$

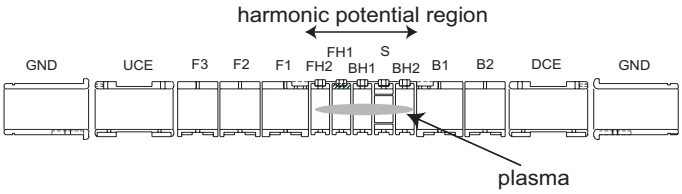

FIGURE 2. The schematic view of the MRT. The electrode "S" is segmented azimuthally.

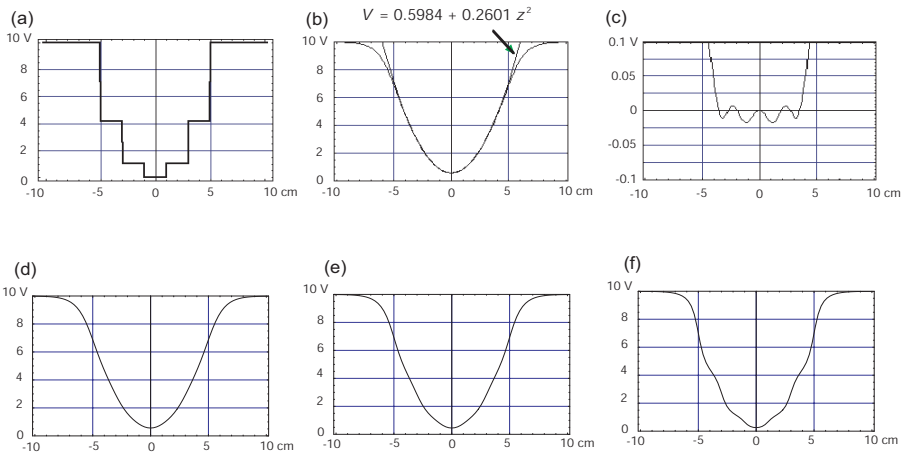

FIGURE 3. (a) Applied voltages on each ring electrode. (b) The produced potential at $\rho = 0$ mm. Fitted quadratic function is also shown. (c) Difference between the produced potential and the quadratic function in the case of (b). (d) $\rho = 5$ mm, (e) $\rho = 10$ mm, (f) $\rho = 15$ mm.

is produced, which is described in the cylindrical coordinate, where the radius of the ring electrode is $R = 20$ mm, the axial length of the trap region is $2L = 125$ mm, the potential difference is $V_0 = \phi(0,L) - \phi(0,0)$ the offset from the surface potential on the center electrode "BH1" is δ. Figure 3 (b) shows the resultant potential along the axis for $V_0 = 10$ V. The quadratic function is superimposed on the produced potential, which is called as harmonic potential. The difference between the produced potential along the axis and the quadratic function is shown in (c). The harmonic potential region is much larger than usual Penning traps. The calculated produced potential at $\rho = 5$ mm, 10 mm and 15 mm are shown in Fig.3 (d), (e), and (f), respectively. As is expected, the produced potential distorted at the larger ρ. During the following experiment, V_0 was chosen to 50 V.

One of the ring electrodes ("S" in Fig. 2) was azimuthally segmented into 4 sectors so that an rf field could be applied to compress the charged particle cloud in the MRT [11].

Electrons as a coolant were injected from the downstream side of the MRT. They were emitted from a field emission array cathode on a pneumatic type feedthrough, which

was retracted during the extraction procedure of ultraslow beams. The typical number of stored electrons was 3×10^8.

Plasma diagnosis

A well cooled charged particle cloud behaves as a nonneutral plasma in an electromagnetic trap. The shape of a plasma confined in a harmonic potential is spheroid under an equilibrium condition, a rigid rotor equilibrium [12]. For diagnosis of the trapped electron plasma, a white noise was applied to the plasma via one of the electrodes comprising harmonic potential region. The excited axially symmetric electrostatic oscillation, (l,0) mode, indicating a number l which corresponds to $l-1$ nodes of the charge distribution along the axial direction of the plasma and a number 0 for azimuthal direction can be observed via another ring electrode. The signal of the oscillation was monitored by a real time spectrum analyzer after amplification. These oscillation induced peaks in the power spectrum at the corresponding mode frequencies. The shift of these peaks with time was used to monitor the antiproton cooling process because these modes has temperature dependence as is discussed in following paragraphs.

The dispersion relation of axially symmetric electrostatic oscillation of cold spheroidal plasmas whose angular frequency ω_l is given by D.H.E. Dubin [13] as

$$\frac{\varepsilon_3}{\varepsilon_0} = 1 - \frac{\omega_p^2}{\omega_l^2} = \left(\frac{\alpha - \varepsilon_3/\varepsilon_0}{\alpha^2 - 1} \right)^2 \frac{P_l(\xi_1) Q_l'(\xi_2)}{P_l'(\xi_1) Q_l(\xi_2)}, \tag{2}$$

where ε_3 is the dielectric tensor element along the magnetic field, ε_0 is the vacuum dielectric constant, a is the radius of the spheroid, $2b$ is the length of the plasma, $\alpha = b/a$ is the aspect ratio, and $\omega_p = \sqrt{n_e q^2/\varepsilon_0 m_e}$ is the angular frequency of the plasma oscillation. Here n_e is the number density of the electrons, q is the electron's charge, and m_e is the mass. P_l and Q_l represent Legendre functions of the first and second kinds, while P_l' and Q_l' denote their derivatives where $\xi_1 = \alpha(\alpha^2 - \varepsilon_3/\varepsilon_0)^{-1/2}$ and $\xi_2 = \alpha(\alpha^2 - 1)^{-1/2}$. Even when the temperature of the plasma, T_e, is finite, but still the boundary of the plasma is regarded as sharp, Eq. 2 is extended to a finite temperature region as [14, 15],

$$\frac{\varepsilon_3}{\varepsilon_0} = 1 - \frac{\omega_p^2}{\omega_l^2} \left(1 + \frac{3 k_B T_e}{m_e} \frac{k^2}{\omega^2} \right) = \left(\frac{\alpha - \varepsilon_3/\varepsilon_0}{\alpha^2 - 1} \right)^2 \frac{P_l(\xi_1) Q_l'(\xi_2)}{P_l'(\xi_1) Q_l(\xi_2)}, \tag{3}$$

where $k = \pi(l-1)/2b$ is the wave number of the electrostatic wave.

The asterisks plotted in Fig. 4 show the observed frequencies of (l,0) modes (l = 1–7). These observed frequencies were fitted by a calculated values (circles in the figure). Under an assumption of thermally stabilized plasma in the 50 V harmonic potential and the length of trapping region $L = 12.5$ cm for 3×10^8 electrons, the mode frequencies of the plasma was calculated as circles shown in Fig.4, which indicated the radius of the plasma was 5.0 mm.

When ω_l of the plasma is experimentally determined for more than two different ls, Eq. 2 gives the density and the aspect ratio. Table 1 shows the observed mode frequencies

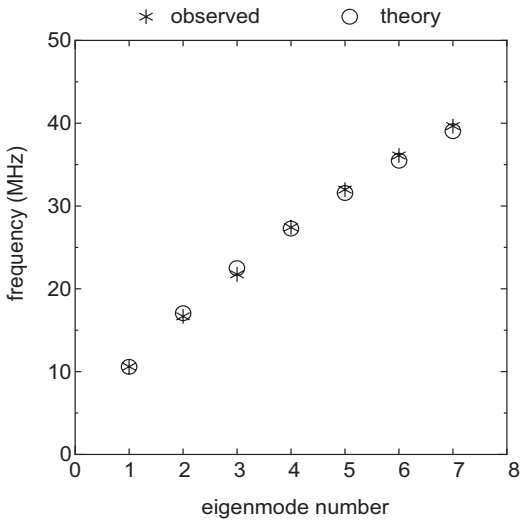

FIGURE 4. Observed and calculated axially symmetric frequencies up to 7th eigenmode.

TABLE 1. Observed frequencies and estimated aspect ratio and density of the electron plasma from two different frequencies. The size of the plasma, *a* and *b*, is also shown, which is evaluated by using independently measured total number of the electron.

$f_{(2,0)}$ [MHz]	$f_{(3,0)}$ [MHz]	$f_{(4,0)}$ [MHz]	aspect ratio	density [/cm^3]	a [mm]	b [mm]
17.660	23.212	–	14	1.2×10^8	3.4	4.6
17.660	–	27.966	13	1.1×10^8	3.6	4.6
–	23.212	27.966	12	1.0×10^8	3.7	4.5

for $l = 2$, 3, and 4. From the relation between two different modes, the aspect ratio and the number density of the plasma was estimated. According to the total number of particles of the plasma which was measured independently, the real size of the plasma, *a* and *b*, can be determined.

Figure 5 shows an example of the time evolution of the power spectrum by the antiproton beam injection where the resonance corresponding to the (1,0), (2,0), and (3,0) modes are clearly observed. The resonance frequency of the (1,0) mode was almost constant for the whole period monitored as is expected from Eq.3. The (2,0) and (3,0) modes increased after the antiproton injection, reached a maximum in a few seconds, and then slowly returned to the initial frequencies. It took about 30 s. Such a frequency variation is due to heat-up of the electron plasma by the antiproton injection followed by the cooling with synchrotron radiation.

These frequency shifts and time evolution were understood from a model considering a beam cooling by a plasma described in Ref. [16]; The energy transfer rate from the

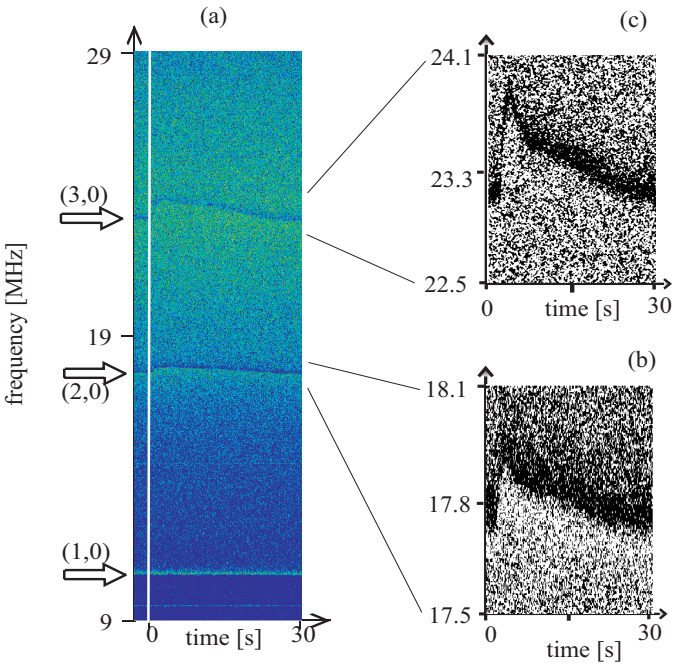

FIGURE 5. (a) Time evolution of the power versus frequency spectrum of the electron plasma after antiproton injection at $t = 0$. The three arrowed regions correspond to the (1,0), (2,0), and (3,0) modes, respectively; (b) and (c) show the (2,0) and (3,0) modes with expanded vertical scales.

antiproton beam to the electron plasma is given by [16],

$$\left\langle \frac{d\mathscr{E}}{dt} \right\rangle = A \frac{n_e q^4 \log\Lambda(T_e, E_{\bar{p}})}{4\pi\varepsilon_0^2 m_e v_{\bar{p}}(E_{\bar{p}})} F\left(\frac{v_{\bar{p}}}{v_e}\right), \tag{4}$$

where the velocities of electron and antiproton are v_e and $v_{\bar{p}}$, respectively. The Coulomb logarithm $\log\Lambda$ is expressed as

$$\log\Lambda(T_e, E_{\bar{p}}) = \log\left(\frac{\lambda_D(T_e)}{L(T_e, E_{\bar{p}})}\right), \tag{5}$$

$$L(T_e, E_{\bar{p}}) = \frac{q^2}{4\pi\varepsilon_0 m_e} \frac{1}{(v_e v_{\bar{p}})^2}, \tag{6}$$

$$\lambda_D = \sqrt{\frac{\varepsilon_0 k_B T_e}{n_e q^2}}. \tag{7}$$

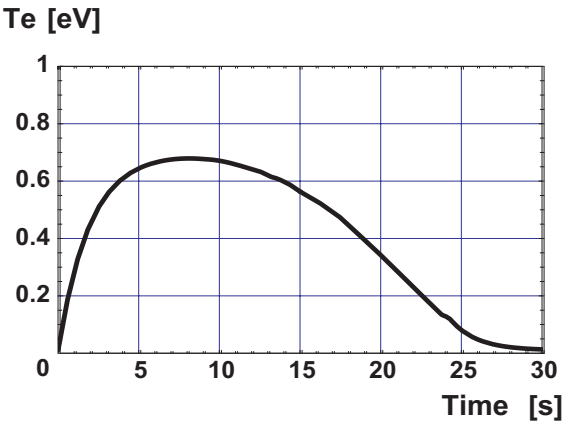

FIGURE 6. Calculated time evolution of the electron plasma temperature.

Here we use the following functions defined as,

$$F(x) = \Phi(x) - \frac{2x}{\sqrt{x}}\left(1 + \frac{m_e}{m_{\bar{p}}}\right)\exp(-x^2), \tag{8}$$

where

$$\Phi(x) = \frac{2}{\sqrt{\pi}}\int_0^x \exp(-t^2)dt, \tag{9}$$

is the error function.

The antiproton beam emerging from the degrader foils is not a monochromatic beam. In this experimental condition, the diffusing time from the velocity perpendicular to the magnetic field $v_\perp$ to the parallel component $v_\parallel$ is much long compared with the deceleration time along the field. For $E_{\bar{p}} = 10$ keV, the diffusion time becomes c.a. 10^4 s, while the deceleration time is the order of 10 s. Therefore we estimate the energy deposit of the antiproton beam to the electron plasma by considering only the energy distribution along the magnetic field axis which experimentally obtained [17]. For simplicity, interactions among antiprotons are also neglected. Considering the experimentally obtained synchrotron radiation cooling time, $\tau_c[\mathrm{s}] \sim 8.6/B[\mathrm{T}]^2$, the energy transfer between the beam to the plasma is found by solving the following simultaneous equation with respect to time t:

$$\frac{dE_{\bar{p}}(t)}{dt} = -\left\langle \frac{d\mathscr{E}}{dt} \right\rangle, \tag{10}$$

$$\frac{dT_e(t)}{dt} = \frac{2}{3k_B}\left(\frac{N_{\bar{p}}}{N_e}\right)\left\langle \frac{d\mathscr{E}}{dt} \right\rangle - \frac{T_e(t)}{\tau_c}, \tag{11}$$

with initial value of $E_{\bar{p}}(0)$ and $T_e(0)$.

The temperature of the electron plasma was evaluated from the frequency shift. The (2,0) and (3,0) mode frequency shift after the antiproton injection were around 0.6 eV and 0.8 eV at the maximum, respectively. Figure 6 shows a calculated time evolution of the electron plasma temperature, which shows the estimated maximum temperature rise was about 0.7 eV. The shift came back to the initial temperature within 30 s. These features by numerically solving the simultaneous Eqs. 10 and 11 agreed with experimental results shown in Fig. 5. Here the coupling constant was chosen to 0.073.

Radial (de)compression

It is known that a rotating rf field can give a torque for confined plasma which is in a rigid rotor equilibrium, and so the radial distribution of the plasma is controlled [18, 19, 20]. In this experiment, the electron plasma was successfully compressed radially by rotating electric dipole field whose frequency and amplitude were around 1–10 MHz and 0.8 V_{pp}. We found that the counter-rotating electric dipole fields rotating inversely against the direction of rigid rotation of the plasma expanded the plasma radially. The parameters of the counter-rotating field were the same as for compression except for the rotation direction. After the expansion, the radius of the plasma was estimated by using Eqs. 2 and 3 with two different electrostatic mode frequencies as described in the above section. By applying the counter-rotating field, the initially formed electron plasma has the radius of 0.7 mm was expanded to 1.7 mm for 15 s counter-rotation, 2.1 mm for 30 s, 3.4 mm for 60 s, and 4.9 mm for 120 s, respectively, as summarized in Tab. 2.

Filled circles in Fig.7 show the number of confined antiprotons as a function of electron plasma radius. This result shows that the injected antiproton beam was broader than the initial electron plasma, that is, without any radial distribution control a considerable amount of injected antiprotons which were not cooled and trapped in the trapping region were lost. The other result by a beam profile monitor located on the entrance of the MRT ("BPM" in Fig. 1) also confirmed that the injected antiproton beams from the RFQD had a larger radius (Fig. 8). From the confined number of antiprotons against radii of plasmas, we roughly estimated the injected antiproton beam profile. Figure 9 shows an example of contained antiproton number within each shell under the assumption that the radial distribution of cooled antiprotons by collisions with the electrons was same as the electron plasma radius, which agrees with the result of the beam profile monitor.

Triangle symbols in Fig. 7 show the extracted number of antiprotons after the electron cooling after the electron release from the trap region[10]. When the radius of the

TABLE 2. Observed frequencies for different radii of plasmas controlled by rotating electric fields.

$f_{(2,0)}$ [MHz]	$f_{(3,0)}$ [MHz]	aspect ratio	radius [mm]	half length [mm]	density [/cm^3]
17.669	24.034	~ 89	~ 0.7	62	$\sim 2.7\times10^9$
17.882	23.949	30	1.7	51	4.2×10^8
17.760	23.689	24	2.1	50	3.0×10^8
17.660	23.212	14	3.4	49	1.2×10^8
17.561	22.756	9	4.9	45	6.5×10^7

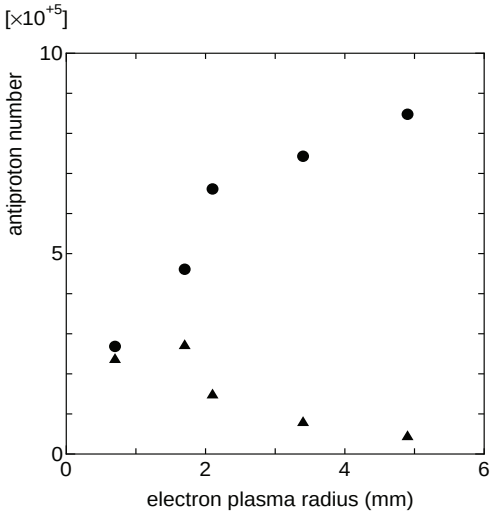

FIGURE 7. Confined antiproton number against the radii of the electron plasmas shown as filled circles. Also extracted number of antiprotons is shown as filled triangles.

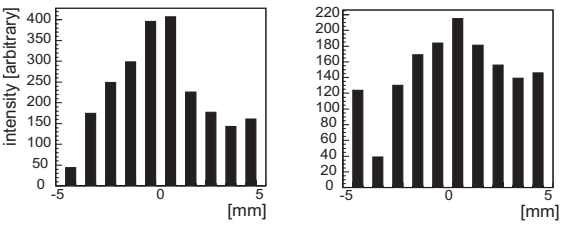

FIGURE 8. An example of the incident antiproton beam profile at the entrance of the MRT.

electron plasma was 1 mm, most of confined antiprotons were extracted as we expected from our beam line design, that is, antiprotons within 1 mm from the axis of the beam line were completely extracted [8]. But for larger radii of plasmas, the extraction numbers of antiprotons were decreased. For example, from the result shown in Fig. 7, smallest size electron plasma whose radius was about 0.7 mm confined and cooled only 2.7×10^5 antiprotons, but most of the cooled antiprotons, that is, 2.3×10^5, were extracted out of the field free region. On the other hand, about 10 mm diameter electron plasma cooled more than 8.0×10^5 antiprotons, but only less than 5×10^4 antiprotons were extracted.

To increase the extraction number of the antiproton, the radial compression technique of antiproton cloud was developed. Before the antiproton cloud compression, electrons were removed from the trapping region by opening and closing the trapping potential well for 550ns three times. Then the antiproton cloud was successfully compressed

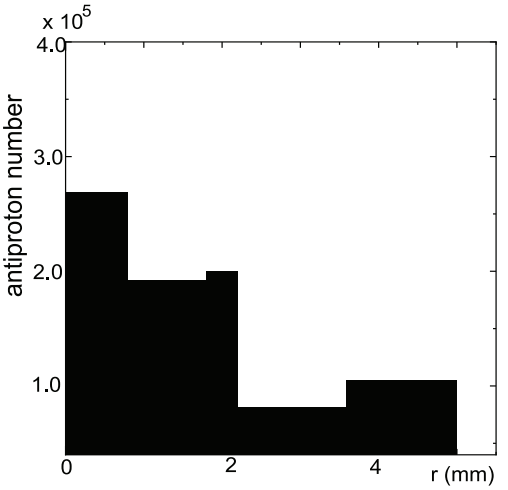

FIGURE 9. An example of the profile of an injected antiproton beam.

radially and extracted out of the field free region.

SUMMARY

The antiprotons passing through the isolation foils were cooled and confined in the harmonic potential provided by the MRT. The cooling process was nondestructively observed by monitoring electrostatic mode frequencies of the electron plasma. This feature was understood by the model considering the beam cooling by the electron plasma and the synchrotron radiation cooling of the electrons in the 2.5 T magnetic field.

The radial distribution of the electron plasma was controlled by utilizing the rotating electric field technique. The injected antiproton beams with large radius were cooled by the expanded electron plasma decompressed by the counter-rotating field against the rigid rotation direction of the electron plasma.

ACKNOWLEDGMENTS

This work was supported by the Grant-in-Aid for Creative Scientific Research (10P0101) of the Japanese Ministry of Education, Culture, Sports, Science and Technology (MonbuKagaku-shō), Special Research Projects for Basic Science of RIKEN, and the Hungarian National Science Foundation (OTKA T033079).

REFERENCES

1. Y. Yamazaki, *Nucl. Instrum. Methods Phys. Res. B*, **154**, 174 (1999).
2. M. Hori, J. Eades, R. Hayano, T. Ishikawa, J. Sakaguchi, E. Widmann, H. Yamaguchi, H. Torii, B. Júhasz, D. Horváth, and T. Yamazaki, *Phys. Rev. Lett.*, **87**, 093401 (2001).
3. H. Knudsen, U. Mikkelsen, K. Paludan, K. Kirsebom, S. P. Møller, E. Uggerhøj, J. Slevin, M. Charlton, and E. Morenzoni, *Phys. Rev. Lett.*, **74**, 4627 (1995).
4. A. Trzińska, J. Jastrzębski, P. Lubiński, F. Hartmann, R. Schmidt, T. von Egidy, and B.Kłos, *Phys. Rev. Lett.*, **87**, 082501 (2001).
5. M. Wada, Y. Ishida, T. Nakamura, Y. Yamazaki, T. Kambara, H. O. ad Y. Kanai, T. Kojima, Y. Nakai, N. Oshima, A. Yoshida, T. Kubo, Y. Matsuo, Y. Fukuyama, K. Okada, T. Sonoda, S. Ohtani, K. Noda, H. Kawakami, and I. Katayama, *Nucl. Instrum. Methods Phys. Res. B*, **204**, 570 (2003).
6. A. Mohri, and Y. Yamazaki, *EuroPhys. Lett.*, **63**, 207 (2003).
7. A. Mohri, H. Higaki, H. Tanaka, Y. Yamazawa, M. Aoyagi, T. Yuyama, and T. Michishita, *Jpn. J. Appl. Phys.*, **37**, 664 (1998).
8. K. Yoshiki Franzen, N. Kuroda, H.A. Torii, M. Hori, Z. Wang, H. Higaki, S. Yoneda, B. Juhász, D. Horváth, A. Mohri, K. Komaki, and Y. Yamazaki, *Rev. Sci. Instrum.*, **74**, 3305 (2003).
9. G. Gabrielse, X. Fei, L. Orozco, R. Tjoelker, J. Haas, H. Kaliowsky, T. Trainor, and W. Kells, *Phys. Rev. Lett.*, **63**, 1360 (1989).
10. N. Kuroda, H.A. Torii, K. Yoshiki Franzen, Z. Wang, S. Yoneda, M. Inoue, M. Hori, B. Júhasz, D. Horváth, H. Higaki, A. Mohri, J. Eades, K. Komaki, and Y. Yamazaki, *Phys. Rev. Lett.*, **94**, 023401 (2005).
11. H. Higaki, N. Kuroda, K. Yoshiki Franzen, Z. Wang, M. Hori, A. Mohri, K. Komaki, and Y. Yamazaki, *Phys. Rev. E*, **70**, 026501 (2004).
12. R. C. Davidson, *PHYSICS OF NONNEUTRAL PLASMAS*, Imperial College Press and World Scientific, London, 2001.
13. D. Dubin, *Phys. Rev. Lett.*, **66**, 2076 (1991).
14. M. Tinkle, R. Greaves, C. Surko, R. Spencer, and G. Mason, *Phys. Rev. Lett.*, **72**, 352 (1994).
15. H. Higaki, N. Kuroda, T. Ichioka, K. Yoshiki Franzen, Z. Wang, K. Komaki, and Y. Yamazaki, *Phys. Rev. E*, **65**, 046410 (2002).
16. D. Sivukhin, "COULOMB COLLISIONS IN A FULLY IONIZED PLASMA," in *Review of Plasma Physics*, edited by A. M. Leontovich, Consultants Bureau, New York, 1966, vol. 4.
17. H. Torii, N. Kuroda, M. Shibata, Y. Nagata, D. Barna, M. Hori, J. Eades, A. Mohri, K. Komaki, and Y. Yamazaki, "Production of ultra-slow antiproton beams," in *Workshop on Physics with Ultra Slow Antiproton Beams*, RIKEN, AIP, 2005 (in press).
18. X.-P. Huang, F. Anderegg, E. Hollmann, C. Driscoll, and T. O'Neil, *Phys. Rev. Lett.*, **78**, 875 (1997).
19. F. Anderegg, E. Hollmann, and C. Driscoll, *Phys. Rev. Lett.*, **81**, 4875 (1998).
20. T. Ichioka, *Development of intense beam of ultracold antiprotons*, Ph.D. thesis, University of Tokyo (2001).